AGU ADVANCING EARTH AND SPACE SCIENCES

Geophysical Research Letters

RESEARCH LETTER
10.1029/2025GL118553

Short-Term Variability of Jupiter's Satellite Footprints as Spotted by JWST

Katie L. Knowles[1], H. Melin[1], T. S. Stallard[1], L. Moore[2,3], J. O'Donoghue[4], C. Schmidt[2,3], J. R. Szalay[5], P. I. Tiranti[1], K. Roberts[2], R. E. Johnson[6], and E. M. Thomas[1]

[1]School of Engineering, Physics & Mathematics, Northumbria University, Newcastle-upon-Tyne, UK, [2]Department of Astronomy, Boston University, Boston, MA, USA, [3]Center for Space Physics, Boston University, Boston, MA, USA, [4]Department of Meteorology, University of Reading, Reading, UK, [5]Department of Astrophysical Sciences, Princeton University, Princeton, NJ, USA, [6]Department of Physics, Aberystwyth University, Aberystwyth, UK

Key Points:

- First near-infrared spectral observations of the auroral footprints of Io and Europa with derived H_3^+ emissions, temperatures, and densities
- Io's main Alfvén wing (MAW) spot exhibits cool H_3^+ temperatures of 538 K, with densities exceeding those in the northern aurora by 3 times
- The extreme observed variability implies short-term changes in the incident electron flux and energy, localized to the MAW spot's center

Supporting Information:

Supporting Information may be found in the online version of this article.

Correspondence to:

K. L. Knowles,
k.knowles@northumbria.ac.uk

Citation:

Knowles, K. L., Melin, H., Stallard, T. S., Moore, L., O'Donoghue, J., Schmidt, C., et al. (2026). Short-term variability of Jupiter's satellite footprints as spotted by JWST. *Geophysical Research Letters*, *53*, e2025GL118553. https://doi.org/10.1029/2025GL118553

Received 29 JUL 2025
Accepted 16 FEB 2026

Author Contributions:

Formal analysis: Katie L. Knowles
Investigation: Katie L. Knowles, H. Melin
Supervision: H. Melin, T. S. Stallard
Writing – original draft: Katie L. Knowles
Writing – review & editing: Katie L. Knowles, H. Melin, T. S. Stallard, L. Moore, J. O'Donoghue, C. Schmidt, J. R. Szalay, P. I. Tiranti, K. Roberts, R. E. Johnson

Abstract We present the main Alfvén wing (MAW) spots of Io and Europa as observed by the Near-Infrared Spectrograph onboard the James Webb Space Telescope. These auroral footprint features have been measured previously, but only in emission. Here, the derived ionospheric H_3^+ emission, temperature and column density are reported, as well as CH_4 spectral radiance. At the Io footprint, H_3^+ temperatures are 670–900 K, excluding a spatially confined cold structure (538 ± 17 K), localized to the MAW spot, with high densities ($0.98 \pm 0.43 \times 10^{16}$ m^{-2}). There are suggestions of a similar, less extreme H_3^+ population associated with the Europa footprint. However, temperatures at Io's MAW spot show significant variability within different observational exposures, indicating precipitation energy changes, sampling various regions of the ionosphere's altitudinal temperature profile. This work provides a new window into understanding the auroral processes driven by moon-magnetosphere interactions in the Jovian system.

Plain Language Summary The James Webb Space Telescope (JWST) conducted a clockwise scan around the entire limb of Jupiter, chasing the northern lights, or aurora, as they rotated into view. This dynamic phenomenon is a result of charged particles traveling down magnetic field lines, crashing into the top of the atmosphere, or ionosphere, and causing it to glow. During its scan, JWST captured an extraordinary aspect of Jupiter's aurora, known as the auroral footprints, which are bright emission patterns produced as a result of the interaction between Jupiter's Galilean moons and the space environment surrounding the planet. Here, we present measurements of the physical properties of the auroral footprints of Jupiter's two innermost Galilean moons, Io and Europa, including the local temperature and ionospheric density, in the near-infrared. A never-seen-before low temperature structure was discovered, centered on Io's bright spot of emission, possessing extremely high densities. This is likely driven by extreme changes in the flow of electrons crashing into the upper atmosphere.

1. Introduction

Jupiter's aurorae are the most powerful and continuously observable of any aurorae in the Solar System, and are a manifestation of the coupling between the atmosphere and surrounding space environment. This phenomenon is due to the planet's powerful magnetic field, fast rotation (~10 hr) and neighboring dense plasma environment (Grodent, 2015). The volcanically active moon, Io, has an atmospheric escape rate of $\sim 10^3$ kg s^{-1} (Roth et al., 2025), which produces extended neutral clouds that become ionized to form the permanent and influential Io plasma torus within the magnetosphere (Steffl et al., 2004).

A striking feature of the Jovian aurorae are the emissions associated with the Galilean satellites. Since Jupiter and its magnetic field rotate faster than the orbital motion of these moons, the satellites continuously interact with the magnetospheric plasma which is co-rotating with the field (reviewed by Saur, 2021 and Bonfond & Sulaiman, 2024). This generates Alfvén waves which accelerate charged particles along magnetic field lines through wave-particle interactions (Damiano et al., 2019; Hess et al., 2010; Jones & Su, 2008; Lysak & Song, 2003). These particles then precipitate into Jupiter's atmosphere, producing the *auroral footprints* at the feet of the field lines that electromagnetically connect the local plasma environment close to, and downstream of, the moons to Jupiter's ionosphere (Connerney et al., 1993; Grodent, 2015). They appear as bright spots followed by a fading tail

of emission, and are identifiable in the infrared (Connerney et al., 1993) and ultraviolet/UV (Clarke et al., 1996) due to the ionization of H_2 to produce H_3^+ and excitation of H_2, respectively.

Io is the innermost Galilean moon (5.9 R_J away from Jupiter, 1 R_J = 71,492 km), and its footprint includes a number of features (not limited to): Main Alfvén Wing (MAW) spot, originating from the direct Io-magnetosphere interaction (Bonfond et al., 2008; Saur et al., 2013); trans-hemispheric Electron Beam (TEB) spot, caused by conjugate electron beams from the opposing hemisphere's MAW spot (Bonfond et al., 2009; Hess et al., 2010); an extended tail trailing the MAW spot (Szalay et al., 2020), can possess a swirling pattern and split in two (Mura et al., 2018).

Less is known about Europa's footprint (at 9.4 R_J) due to its weaker emission and the lack of observations with a visible tail (Allegrini et al., 2020; Bonfond et al., 2017; Grodent et al., 2006). It is located at the equatorward edge of the bright main auroral emission (magnetically mapping to 20–30 R_J in the magnetosphere's equatorial plane), and can often be disturbed by injection signatures (Dumont et al., 2014; Hess, Bonfond, & Delamere, 2013). The substructure of the footprint tail appears as sequential periodic sub-dots or a fading arc (Moirano et al., 2021).

The electrodynamic interaction between Jupiter and the Galilean moons results in the acceleration of plasma into the planet's upper atmosphere, creating additional production of H_3^+, a prevalent molecular ion in Jupiter's ionosphere (Achilleos, Miller, Tennyson, Aylward, et al., 1998; Connerney et al., 1993). Its near-infrared (NIR) emissions are governed by its thermal excitation, such that the observed intensity is dependent on both the local ion density and thermospheric temperature (Miller et al., 2013). H_3^+ is formed by the ionization of neutral molecular hydrogen, either via electron precipitation predominately at the magnetic poles, or dayside photoionization. After formation, H_3^+ quickly becomes thermalized to the neutral atmosphere (Miller et al., 2020), thus its derived temperature is a proxy for the local thermospheric temperature. It is primarily destroyed via dissociative recombination with free electrons or through charge-exchange with hydrocarbons, such as methane, beneath the homopause (Moore et al., 2004, Figure 5).

The intricate morphology of moon-induced footprints reflect the complex dynamics of the interaction, allowing us to gain insight on the coupling between Jupiter and the plasma environment at the satellites' orbits, but not on their generation. The precipitating flux will preferentially interact with different atmospheric altitudes depending on their energy (Szalay et al., 2018), and the derived H_3^+ parameters represent a convolution of the vertical density and temperature structure. Therefore, NIR spectral measurements allow constraints to be placed on the precipitation flux, energy and variability, granting unique understanding on the footprints generation and impact on Jupiter's ionosphere. Such work is relevant for NASA's Juno mission (Bolton et al., 2017), as well as to support future investigations of the Galilean moons, including the Jupiter Icy Moons Explorer (Juice) and Europa Clipper.

Here, we detail the spectral measurements taken by the James Webb Space Telescope (JWST) of the NIR footprints of Io and Europa in Section 2, followed by our results in Section 3. A discussion is given in Section 4, before we conclude in Section 5.

2. Observations and Methodology

2.1. Observations

JWST performed observations of Jupiter using the Near-Infrared Spectrograph NIRSpec's Integral Field Unit, IFU (Jakobsen et al., 2022), on 7 September 2023 for a total of 22.18 hr. Thirty-six individual observations were carried out, every 10° in latitude, scanning clockwise around the planet's limb. Each observation consists of 4 dithers (individual exposures taken after small, precise movements made by JWST), totaling 144 dithers, each with 86 s of exposure time. Five dithers captured the Io footprint, progressing poleward from (1) to (5) in Figure 1, with (3)–(5) including the Europa footprint. Observational details are summarized in Table 1.

The IFU produces a 3-dimensional cube with 2 spatial dimensions containing 30 × 30 spaxels (spatial pixel), each measuring 0.1″ × 0.1″, to give a spatial resolution of ∼319 km/spaxel. Using the G395H/F290LP grating/filter setting, the spectral dimension (2.87–5.27 μm), with a resolving power of R ∼2,700, allows us to capture bright H_3^+ emission lines, as well as high-altitude non-local thermal equilibrium (non-LTE) CH_4. The strong sunlight absorption by deep CH_4 renders this wavelength region spectrally free from solar reflectance features from the lower atmosphere.

10.1029/2025GL118553

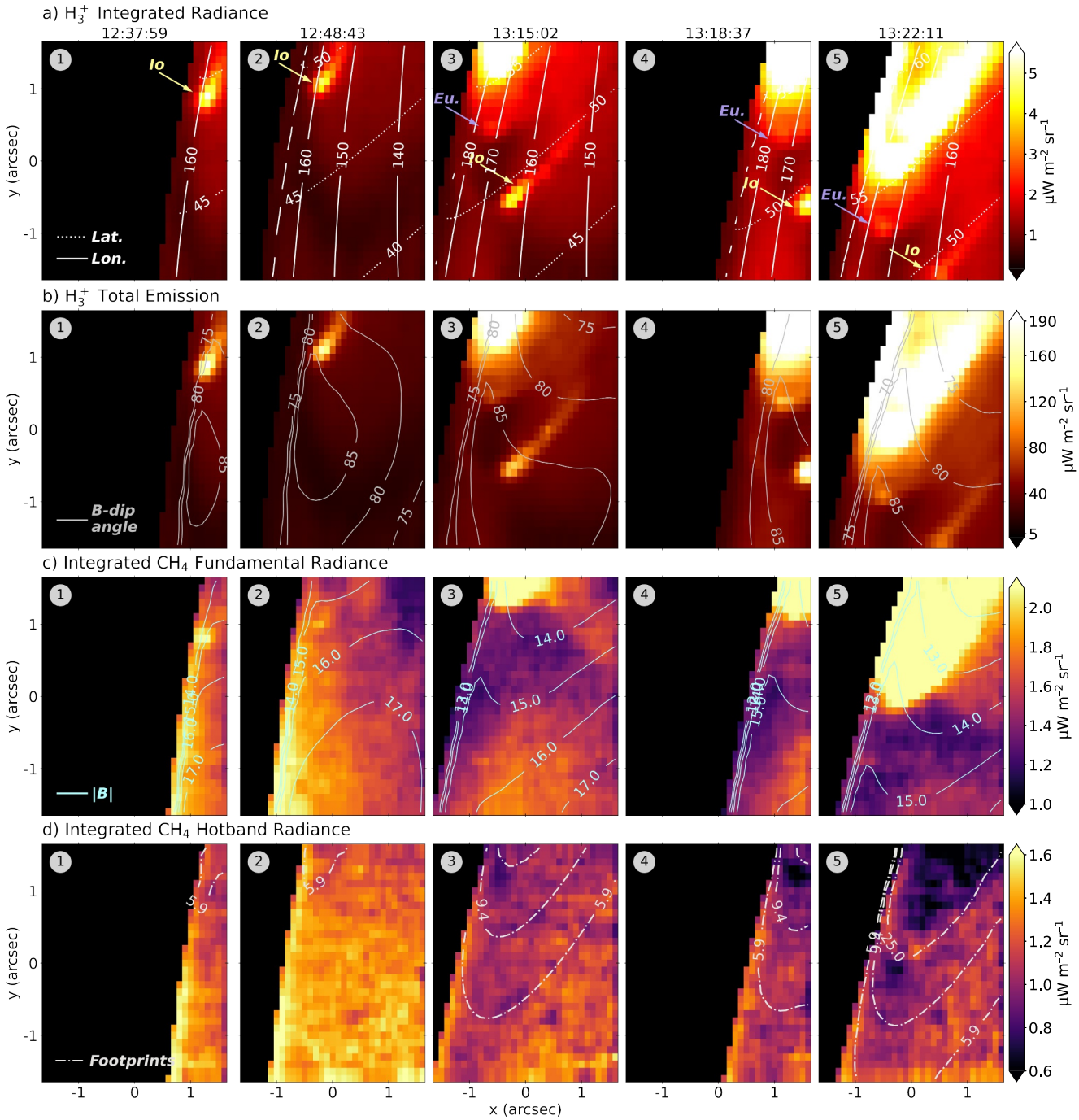

Figure 1. JWST/NIRSpec IFU observations of the auroral footprints of Io and Europa, indicated by yellow and purple arrows, respectively. (a) Integrated H_3^+ radiance with planetocentric latitude at 550 km above the 1-bar level (dotted) and System III (West) longitude (solid). (b) Total H_3^+ emission with dotted gray lines for magnetic dip angle (degrees). (c) Integrated CH_4 fundamental emissions with total magnetic field strength in Gauss (blue dotted) and (d) integrated CH_4 hotband emissions with dash-dotted contours of the magnetic footprints of Io (5.9 R_J), Europa (9.4 R_J) and main auroral oval (25.0 R_J). UTC mid-points are given above.

2.2. Methodology

As in Melin et al. (2024), we approximately model the spectral shape of the non-LTE solar-excited CH_4 emissions between 3.29 and 3.55 μm. Utilizing the HITRAN CH_4 line list (Gordon et al., 2017), the radiance of its 3 components can be modeled; the fundamental, hotband and a third-order polynomial background. The residual between the NIRSpec data and CH_4 model contains the isolated H_3^+ spectrum, which we fit using *h3ppy*

Table 1
Summary of James Webb Space Telescope Observations

Name (& dither #)	UTC midpoint	LON (°W)	LAT (°)	LT (hr)	SUB-IO JOV. LON (°W)
JUPITER-DAWN-L45N (1)	12:37:59	151.8	46.0	7.6	142.9
JUPITER-DAWN-L45N (4)	12:48:43	147.8	44.3	8.3	147.8
JUPITER-DAWN-L55N (2)	13:15:02	156.7	49.3	8.6	160.0
JUPITER-DAWN-L55N (3)	13:18:37	172.2	51.1	7.9	161.7
JUPITER-DAWN-L55N (4)	13:22:11	164.1	53.7	8.6	163.3

Note. LON = median System III longitude, LAT = planetocentric latitude, LT = planetary local time, and SUB-IO JOV LON (sub-Io Jovian longitude) = System III longitude on Jupiter where Io is located relative to the 1-bar level (accounting for light travel time from Jupiter to JWST).

(Melin, 2025). Both the H_3^+ temperature and column density can be retrieved from the spectra, as well as the total H_3^+ emission (a measure of its radiative cooling rate, Miller et al., 2013). Figure S1 in Supporting Information S1 shows spectral fits from the observations.

Both H_3^+ and CH_4 emit across a series of altitudes, hence a longer atmospheric column is measured at the limb due to the planet's curvature (Achilleos, Miller, Tennyson, & Team, 1998). To correct the H_3^+ parameters for the differing observed path-lengths through the atmosphere, we determined the line-of-sight (LOS) path-length along the pointing vector connecting the base of the ionosphere to JWST, and divided by the assumed height of a uniform ionospheric layer (~200 km, Grodent et al., 2001), providing a first-order approximation. This was conceptualized by Johnson et al. (2018), yet we accounted for Jupiter's oblateness (as in Melin, Fletcher, et al., 2025 and Stallard et al., 2025). For CH_4, we apply the correction methodology from Melin, Stallard, et al. (2025).

We compare the H_3^+ parameters to the local magnetic environment by utilizing *JupiterMag* (Wilson et al., 2023) together with the JRM33 internal field model (Connerney et al., 2022, version 1.3.0 using 13 degree harmonics) and Con2020 external field model (Connerney et al., 2020, ran in analytic mode with default parameters). We assumed an oblate spheroid with an equatorial and polar radius of 71,492 and 66,854 km, respectively, with the ionosphere ~550 km above the 1-bar level. Field lines were traced from the ionosphere out to the magnetosphere's equatorial plane to determine its M-shell (i.e., a given non-dipolar field line that crosses the magnetic equatorial plane at a planetary radial distance of M from Jupiter's center).

3. Results

In Figure 1, we present the JWST/NIRSpec observations showing the auroral footprints of Io and Europa in Jupiter's northern hemisphere. Figure 1a shows integrated H_3^+ radiance (emission intensity), and Figure 1b displays H_3^+ total emission with magnetic dip angle (the angle between a given field line and the local "surface"). Figure 1c shows the integrated CH_4 fundamental radiance with the total magnetic field strength, and the integrated CH_4 hotband radiance is presented in Figure 1d. The total integrated CH_4 emissions, and the ratio of the fundamental and hotband components, are in Figure S2 of Supporting Information S1.

The Io MAW spot is either partially or fully visible in dithers (1)–(4) in Figure 1a, and the footprint tail is observable in (3) and (5). The Europa footprint displays no resolvable sub-structure in Figure 1a or Figure 1b in (3)–(5), equatorward of the aurora rotating into view from (3)–(5).

Figure 2 shows the derived H_3^+ temperatures ($T_{H_3^+}$) and column densities ($N_{H_3^+}$) with their associated uncertainties. To investigate the primary driver of the satellite footprints' H_3^+ radiance enhancements, we plot the relationship between the integrated H_3^+ radiance with $T_{H_3^+}$ and $N_{H_3^+}$ in Figure 3. A "blank region" is included for comparison (spatially separated from any emission features). For both footprints, we focus on a spatial region almost entirely filled by the MAW spot to ensure a sufficient number of data points. For Io, we investigate (2) and (3) as they have the closest observing geometry and the MAW spot is fully visible in both, and we use (3) for Europa.

The large-scale region of weaker H_3^+ emissions across all dithers in Figure 1a, extending from ~42° to ~53°N, spatially coincides with an identified darkening (Stallard et al., 2018), dubbed the *Head of the Northern Silhouette*

10.1029/2025GL118553

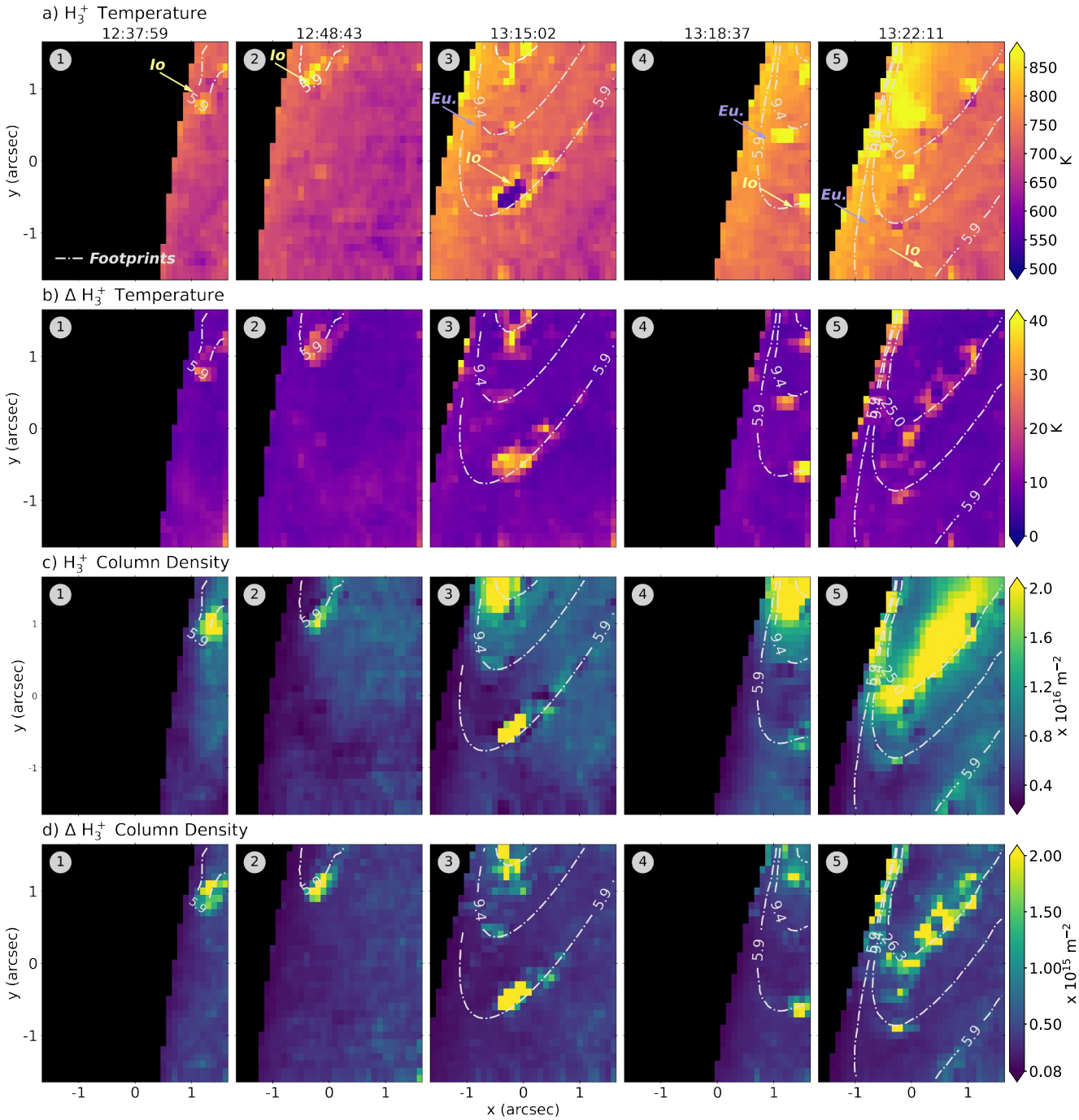

Figure 2. H_3^+ temperature and column density spectral retrievals. (a) H_3^+ temperature, (b) uncertainty of the retrieved temperature, (c) H_3^+ column density, and (d) its uncertainty.

in Knowles et al. (2025). Figure 2 reveals decreased $N_{H_3^+}$ by $\sim 2 \times 10^{15}$ m^{-2} relative to its surroundings, closely following where field lines are near-perpendicular relative to the 1-bar level (Figure 1b). This feature has been attributed to a local $N_{H_3^+}$ reduction, in agreement with our observations, due to the complex field at this location leading to complicated plasma dynamics (Agiwal et al., 2025; Knowles et al., 2025; Roberts et al., 2026; Stallard et al., 2018). Analysis of Jupiter's ionospheric darkening with JWST will be subject of a future study.

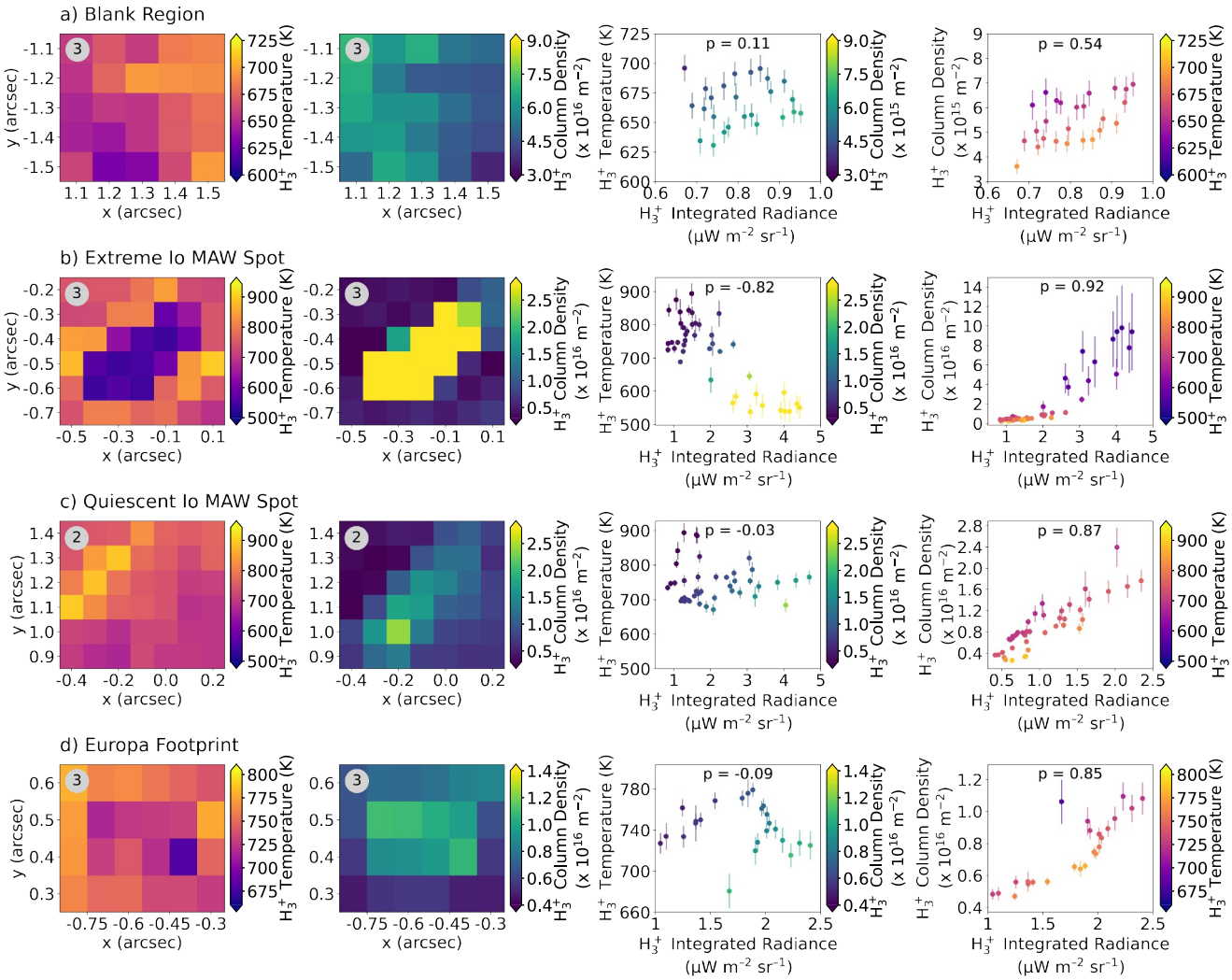

Figure 3. Drivers of H_3^+ radiance. The two leftmost columns show H_3^+ temperature and column density for a spatial location encapsulating (a) "a blank region," Io's main Alfvén wing spot for dithers (b) 3 and (c) 2, and (d) the Europa footprint. The relationship between H_3^+ temperature and radiance, and between the H_3^+ column density and radiance, are displayed in the two right-hand columns, respectively, with uncertainties. *p* indicates the Pearson correlation coefficient.

4. Discussion

4.1. The Io Footprint

Figure 2a shows a spatially confined cold structure, unique to (3) and localized to the core of Io's MAW spot. $T_{H_3^+}$ reaches a minimum of 538 ± 17 K, and is haloed by higher temperatures of 766 ± 14 K, extending into the footprint tail. The ionospheric temperature immediately westward in (3), before the footprint has crossed, is comparable (740 ± 8 K). The $N_{H_3^+}$ associated with the MAW spot reaches a maximum of $9.8 \pm 4.3 \times 10^{16}$ m^{-2}, far exceeding those observed in the main auroral emission ($\sim 3 \times 10^{16}$ m^{-2}). Conversely, the other dithers exhibit an increase in both $T_{H_3^+}$ and $N_{H_3^+}$ at the MAW spot. The significantly different H_3^+ parameters observed in (3) may be due to: (a) the Io footprint traversing through diverse ionospheric/magnetic spatial conditions, (b) the observing geometry revealing the footprint's deeper altitudinal extent, and (c) temporal variations in the electron precipitation due to either local changes in the acceleration process or in the moon-magnetosphere interaction.

In Figure 1, the footprint is rotating through a region where field lines are near-perpendicular relative to the 1-bar level. The field strength is also high (14.0–17.5 G) due to the magnetic feature, *the Northern Hemispheric Flux Band*, at these longitudes (Connerney et al., 2018). The MAW footprint is known to be strongly modulated with

Io's magnetic longitude (Bonfond et al., 2013; Hue et al., 2019; Wannawichian et al., 2013), due to density and magnetic field variations that Io encounters through the torus (Hess, Bonfond, Chantry, et al., 2013). However, the magnetic conditions do not significantly vary across (1)–(5), neither does the footprint's longitudinal position, and the Poynting flux is only expected to change by ∼10% across System III longitudes of 160–180°W (Hess, Bonfond, Chantry, et al., 2013, Figure 3). Therefore, the footprint's traversal through the local magnetic conditions is unlikely to be the primary contributor for the observed phenomenon in (3), but may suggest an intrinsic stochastic variability in the electron precipitation.

We assess whether the driver of the H_3^+ radiance differs between (3), where the low-temperature MAW core is observed, and (2), where it is not seen, in Figures 3b and 3c, respectively. The strongly correlated relationship between $N_{H_3^+}$ and radiance possesses a Pearson correlation coefficient (p) of 0.92 and 0.87 for (3) and (2), respectively. Yet uniquely in Figure 3b, a strong anti-correlation with $T_{H_3^+}$ is introduced ($p = -0.82$), implying the enhanced H_3^+ radiance associated with Io's MAW spot is primarily driven by increased $N_{H_3^+}$, but the precipitation also acts to reduce $T_{H_3^+}$. Furthermore, the $N_{H_3^+}$ across the MAW spot spatially varies by a factor of ∼45 (Figure 3b). By contrast, $N_{H_3^+}$ in Figure 3c vary by ∼9 at the MAW spot, and the $T_{H_3^+}$ variation is comparable between (2) and (3), with a factor of ∼1.3 and ∼1.7, respectively.

The mean emission angle is 74.8° and 81.7° in Figures 3b and 3c, respectively, leading to a 6.9° difference in the viewing geometry. The Io footprint is also close to the limb in (1) and (2). In tandem, these may influence the columns of atmosphere observed, with the Io spot observed the most directly in (3). However, a narrow layer of high-$N_{H_3^+}$, low-$T_{H_3^+}$ at the MAW spot will be always visible since any intervening H_3^+ would be optically thin (and lower density, Lam et al., 1997). Increasing the path-length would have a negligible effect unless neighboring layers possess comparable densities (not observed in Figure 2). Thus, the changing viewing geometry cannot explain the variability across different exposures.

The increased $N_{H_3^+}$ could be losing energy to space via its thermal infrared emissions, thus cooling the atmosphere through the H_3^+ thermostat effect (Miller et al., 1994, 2010). The power (P) required to cool the atmosphere, in the absence of horizontal transport, to the derived temperatures for the MAW spot would be

$$P = \frac{c_p \Delta T}{\Delta t}, \tag{1}$$

where c_p is the total heat capacity of the gas, ΔT is the temperature change and Δt is the time when ΔT occurs. Using the methodology in Melin et al. (2006), we utilize $\Delta t = 1$ hr (timing between start of dither 1 and end of dither 5) and $\Delta T = 218$ K (temperature difference between MAW core and surroundings in dither 3). Assuming LTE, the total work required to cool the atmosphere is 0.97 $Wm^{-2}sr^{-1}$, whereas the total emission (its cooling rate) from Figure 1b is ∼100 $\mu Wm^{-2}sr^{-1}$. Therefore, the H_3^+ cooling effect cannot explain the temperature structure in (3), given that the required energy loss to cool the atmosphere is $\sim 1 \times 10^5$ larger than what the H_3^+ cooling provides.

A bright, cool and dense population of H_3^+ at the MAW spot may sit at lower altitudes relative to its surroundings, where temperatures are cooler (Migliorini et al., 2019; Moore et al., 2019). Changeable electron energies could produce H_3^+ at different altitudes, sampling various regions of the upper atmosphere's vertical temperature profile. Using Figure 2a and the Jovian temperature vertical profile from Tao et al. (2011), we calculated the altitude at which the observed $T_{H_3^+}$ occurs above the 1-bar level (Figure S3 in Supporting Information S1). Within (3), the H_3^+ ions at the MAW core are predicted to reside around 400 km, corresponding to a H_3^+ production rate caused by auroral electrons with energies of 10–100 keV (Tao et al., 2011) or 10–20 keV (Gérard et al., 2014). For the halo population, and the Io footprint in the other dithers, the H_3^+ sits at 600–650 km (≤10 keV).

If the incident electrons are able to propagate beyond the base of the ionosphere, they may affect lower-altitude CH_4. An enhancement in the CH_4 emissions can indicate local heating or an elevated homopause altitude. If there is no spatial variation in the CH_4 emissions at the MAW spot, either the electrons are not energetic enough, or any excitation is relatively minor (Sánchez-López et al., 2021). Furthermore, since the fundamental band sits at higher altitudes than the hotband (Sánchez-López et al., 2021), the component emissions may help characterize precipitation depth.

In Figure 1c, the fundamental CH_4 emissions show a faint enhancement at the MAW spot, unique to (1) and (2), but there is no corresponding brightening in the hotband (Figure 1d). Figure S2 in Supporting Information S1 shows a weak enhancement in the component ratio for (1)–(4) at the location of the MAW spot. This may be explained by the faint brightening in the fundamental (dithers 1 and 2 in Figure 1c), whereas for dithers (3) and (4), it may be tentatively attributed to a minor reduction in the hotband (Figure 1d). However, the weaker hotband emissions at the MAW spot are relatively indistinguishable from the noise within Figure 1d, owing to its lower signal-to-noise. Consequently, Figure 1 and Figure S2 in Supporting Information S1 suggest the Io footprint causes a minor signature in the CH_4 fundamental radiance that can only be seen at the limb due to the LOS enhancement (hence it is not observed in dithers 3–5), and/or the energetic flux affecting (3) is not significant enough to reach the CH_4.

The Io-Jupiter interaction can generate large enhancements in ionospheric density, likely affecting the conductivity and hence governing the currents flowing between them (Gérard et al., 2020). The observed $T_{H_3^+}$ in Figure 2a indicate a change in the peak ionization altitude across the MAW spot, implying an energy variation in the precipitation, and the extreme variability in $N_{H_3^+}$ suggests short-term temporal variations in the incident flux (Figure 2c). Considering the range of $N_{H_3^+}$ across the Io footprint and over each dither, and thus the variability in H_3^+ production, on the timescales of 1.4 min (integration time) and 3.5 min (timing between dithers), the electron flux (and likely energy) changes may be on similar timescales. Further, since the footprint traverses across longitudes such that precipitation cannot act on a parcel of atmosphere for an extended period, the H_3^+ at the MAW core is presumably short-lived. Mura et al. (2025) derived a H_3^+ lifetime of hundreds of seconds in the Io spot (dependent on $N_{H_3^+}$) using measurements acquired by Juno's Jovian Infrared Auroral Mapper (JIRAM, Adriani et al., 2017).

The inferred electron energies indicate values of 10–100 keV (Tao et al., 2011) and 10–20 keV (Gérard et al., 2002, 2014), and JIRAM measurements suggest 10 keV incident electrons at the Io footprint (Mura et al., 2025). Using Juno Ultraviolet Spectrograph observations (Gladstone et al., 2017), Moirano et al. (2026) derived a mean electron energy of 13 keV for Io's MAW spot during perijove (orbit) 40, with significant variability between perijoves. For the footprint tail in (3), we infer incident energies of ∼10 keV (Tao et al., 2011) and <5 keV (Gérard et al., 2014), which are slightly larger than the 1.1 and 0.4–3 keV mean energies from Bonfond et al. (2009) and Moirano et al. (2026), respectively. However, these estimated altitudes, and subsequent electron energies, are model-dependent, and the use of alternate atmospheric models will yield different values. Juno's Jovian Auroral Distributions Experiment (JADE, McComas et al., 2017) often does not register statistically significant electron counts above 10 keV, and there have been few passes through the MAW flux tube. Nonetheless, there are isolated instances in which precipitating electrons of ≥10 keV are observed on ∼1 s timescale (Szalay et al., 2020, Figure 1c). The total energy flux varied by approximately an order of magnitude, implying fine structure to the electron fluxes, consistent with our interpretation of highly variable precipitation. Additionally, during the JWST observations, the TEB spot was expected to be close to, perhaps overlapping, with the MAW spot, which may contribute to the influx of energetic electrons.

Moirano et al. (2023) detected variability in the footprint's position, related to changes in the plasma conditions about Io's orbit, which may have subsequent effects on the footprint's ionospheric structure. Changes in the UV brightness have also been highlighted on ∼1 min (Bonfond et al., 2007) and 2–4 min (Bonfond et al., 2013) timescales, possibly indicating variable mean electron energies, and are comparable to the JWST timings (∼1.4 and ∼3.5 min). Ultimately, we are unable to decipher the mechanism responsible for short-term temporal variations in the precipitation. Likewise, we cannot establish how it may be modified by planetary local time, Io's location within its torus, or the ionospheric magnetic conditions. Additional observations need to constrain whether the examined data represents the "typical" spectral variability, and how it varies, since our observations represent single snapshots in time and space.

4.2. The Europa Footprint

The footprint of Europa, the smallest Galilean moon, displays a faint enhancement in the H_3^+ integrated radiance and total emission (Figure 1, dithers 3–5). Additional observations are shown in Figures S4–S6 in Supporting Information S1, labeled (6)–(8). We exclude (4) and (5) from further discussion due to bad spaxels giving non-physical values at the Europa auroral footprint.

The footprint has no significant enhancements in the CH_4 emissions (Figure 1, Figures S4 and S5 in Supporting Information S1), and no compelling spatial variations in $T_{H_3^+}$ (Figure 2a and Figure S6a in Supporting

Information S1). The calculated altitude at which the derived temperature occurs for the footprint is ∼530 km (Figure S3 in Supporting Information S1), implying electron energies of 5–10 keV (Gérard et al., 2014; Tao et al., 2011) that are comparable to in situ measurements (Allegrini et al., 2020).

The $N_{H_3^+}$ are around $9.0 \pm 0.6 \times 10^{15}$ m^{-2} in both Figure 2c and Figure S6c in Supporting Information S1, and Figure 3d shows how its H_3^+ radiance is well correlated with $N_{H_3^+}$ ($p = 0.85$). A distinct outlier possesses relatively low $T_{H_3^+}$ and high $N_{H_3^+}$ in Figure 3d, potentially indicative of a cold, dense population of H_3^+ associated with the footprint aurora, as has been observed for Io. However, this is based on a single spaxel with large uncertainties, which makes it statistically challenging to conduct further analysis.

5. Conclusions

We analyze the first NIR spectral measurements of the auroral footprints of Io and Europa from JWST NIRSpec IFU observations, and reveal how they alter Jupiter's sub-auroral ionosphere. The H_3^+ radiance for both footprints is predictably found to be primarily driven by column density, as opposed to the local thermospheric temperature, but has not been directly observed until now.

Significant variability is detected in the H_3^+ temperatures (∼40%) and densities (∼310%) across ∼23 min at the center of Io's MAW spot, and is presumably driven by changes in the precipitation flux and energy. A cold core of high density H_3^+ was seen within the Io footprint, surrounded by a relatively hot "halo" extending into the footprint tail, and is indicative of the sensing of two populations, partitioned in altitude. This never-seen-before feature likely requires energetic electron precipitation to generate a high concentration of ionospheric H_3^+, with production occurring at higher (warmer) altitudes encircling it. Therefore, we have revealed the 2-dimensional structure of the incident electrons at Io's auroral footprint.

Our findings highlight the unique insights gained from analyzing the NIR spectra from the footprints of Jupiter's Galilean moons, where it is possible to constrain their variability and infer the plasma properties about the satellites' orbits. The high derived H_3^+ column density and implied production rate will provide useful constraints for models. This analysis, as well as future endeavors, can supply context to in situ measurements acquired by Juno as it traversed within the moons' orbits during its prime and extended missions, as well as for Juice and Europa Clipper.

Conflict of Interest

The authors declare no conflicts of interest relevant to this study.

Data Availability Statement

JWST GO program #3665 NIRSpec IFU observations of Jupiter are publicly available at https://doi.org/10.17909/vjrd-5x14. The data which supports the JRM33 field model are archived using the NASA Planetary Data System at https://doi.org/10.17189/1519711 (Connerney, 2017), and the data set supporting the Con2020 current sheet model can be found within the NASA Planetary Data System at https://pds-ppi.igpp.ucla.edu/search/default.jsp. The open-source python package, *JupiterMag*, used to utilize both the JRM33 and Con2020 models can be found at https://github.com/mattkjames7/JupiterMag.git (where the corresponding journal article is at https://doi.org/10.1007/s11214-023-00961-3). The *h3ppy* H_3^+ modeling and fitting code is on GitHub at https://github.com/henrikmelin/h3ppy (and the associated journal article is at https://doi.org/10.21105/joss.07536).

Acknowledgments
This work is based on observations with the NASA/ESA/CSA James Webb Space Telescope obtained from the Mikulski Archive at the Space Telescope Science Institute, which is operated by the Association of Universities for Research in Astronomy, Incorporated, under NASA Contract NAS5-03127 (https://archive.stsci.edu/). K.L.K. was supported by a Northumbria University Research Studentship at Northumbria University, UK. H.M. was supported by the STFC James Webb Fellowship (ST/W001527/2) at Northumbria University, UK. T.S.S. and E.M.T. were supported by an STFC Consolidated Grant (ST/W00089X/1) at Northumbria University, UK. Support for L.M. under Program JWST-GO-03665.002-A was provided through a STScI Grant under NASA Contract NAS5-03127. J.O. was supported by the STFC Ernest Rutherford Fellowship ST/X003426/1 at the University of Reading, UK. P.I.T. was funded by STFC Studentship ST/X508548/2. K.R. was supported by NASA FINESST Grant 80NSSC23K1637. R.E.J. was supported by a NERC Grant (NE/W002914/1) at Aberystwyth University, UK. We acknowledge the contribution of the International Space Science Institute (ISSI) for hosting and funding the international team on "Jupiter's Non-Auroral Ionosphere" (23-592), as well as the helpful discussions with fellow team members. Discussions with Imke de Pater in the early phase of the work were also appreciated. The authors wish to thank the two anonymous reviewers for their time, consideration and valuable feedback.

References

Achilleos, N., Miller, S., Tennyson, J., Aylward, A. D., Mueller-Wodarg, I., & Rees, D. (1998). JIM: A time-dependent, three-dimensional model of Jupiter's thermopshere and ionosphere. *Journal of Geophysical Research*, *103*(E9), 20089–20112. https://doi.org/10.1029/98JE00947

Achilleos, N., Miller, S., Tennyson, J., & Team, U. J. G. (1998). Models of Jupiter's auroral electrojet. *Bulletin of the American Astronomical Society*, *30*(1083).

Adriani, A., Filacchione, G., Di Iorio, T., Turrini, D., Noschese, R., Cicchetti, A., et al. (2017). JIRAM, the Jovian infrared Auroral mapper. *Space Science Reviews*, *213*(1–4), 393–446. https://doi.org/10.1007/s11214-014-0094-y

Agiwal, O., Moore, L., Bloch, T., Coffin, D., Felici, M., Knowles, K. L., et al. (2025). Unraveling Jupiter's enigmatic ionosphere: Evidence of magnetically-controlled wind-driven dynamics. *Geophysical Research Letters*, *52*(24), e2025GL119171. https://doi.org/10.1029/2025GL119171

Allegrini, F., Gladstone, G. R., Hue, V., Clark, G., Szalay, J. R., Kurth, W. S., et al. (2020). First report of electron measurements during a Europa footprint tail crossing by Juno. *Geophysical Research Letters*, *47*(18), e2020GL089732. https://doi.org/10.1029/2020GL089732

Bolton, S. J., Adriani, A., Adumitroaie, V., Allison, M., Anderson, J., Atreya, S., et al. (2017). Jupiter's interior and deep atmosphere: The initial pole-to-pole passes with the Juno spacecraft. *Science*, *356*(6340), 821–825. https://doi.org/10.1126/science.aal2108

Bonfond, B., Gérard, J. C., Grodent, D., & Saur, J. (2007). Ultraviolet Io footprint short timescale dynamics. *Geophysical Research Letters*, *34*(6), L06201. https://doi.org/10.1029/2006GL028765

Bonfond, B., Grodent, D., Gérard, J., Radioti, A., Saur, J., & Jacobsen, S. (2008). UV Io footprint leading spot: A key feature for understanding the UV Io footprint multiplicity? *Geophysical Research Letters*, *35*(5), L05107. https://doi.org/10.1029/2007GL032418

Bonfond, B., Grodent, D., Gérard, J. C., Radioti, A., Dols, V., Delamere, P. A., & Clarke, J. T. (2009). The Io UV footprint: Location, inter-spot distances and tail vertical extent. *Journal of Geophysical Research*, *114*(A7), A07224. https://doi.org/10.1029/2009JA014312

Bonfond, B., Hess, S., Gérard, J. C., Grodent, D., Radioti, A., Chantry, V., et al. (2013). Evolution of the Io footprint brightness I: Far-UV observations. *Planetary and Space Science*, *88*, 64–75. https://doi.org/10.1016/j.pss.2013.05.023

Bonfond, B., Saur, J., Grodent, D., Badman, S. V., Bisikalo, D., Shematovich, V., et al. (2017). The tails of the satellite auroral footprints at Jupiter. *Journal of Geophysical Research: Space Physics*, *122*(8), 7985–7996. https://doi.org/10.1002/2017JA024370

Bonfond, B., & Sulaiman, A. (2024). Chapter 7 - Alfvén waves related to moon–magnetosphere interactions. In *Alfvén waves across heliophysics: Progress, challenges, and opportunities*. American Geophysical Union. https://doi.org/10.1002/9781394195985.ch7

Clarke, J. T., Ballester, G. E., Trauger, J., Evans, R., Connerney, J. E. P., Stapelfeldt, K., et al. (1996). Far-ultraviolet imaging of Jupiter's aurora and the Io "footprint". *Science*, *275*(5286), 404–409. https://doi.org/10.1126/science.274.5286.404

Connerney, J. E. P. (2017). Juno fluxgate magnetometer calibrated data V1.0 [Dataset]. *NASA Planetary Data System*. https://doi.org/10.17189/1519711

Connerney, J. E. P., Baron, R., Satoh, T., & Owen, T. (1993). Images of excited H_3^+ at the foot of the Io flux tube in Jupiter's atmosphere. *Science*, *262*(5136), 1035–1038. https://doi.org/10.1126/science.262.5136.1035

Connerney, J. E. P., Kotsiaros, S., Oliverson, R. J., Espley, J. R., Joergensen, J. L., Joergensen, P. S., et al. (2018). A new model of Jupiter's magnetic field from Juno's first nine orbits. *Geophysical Research Letters*, *45*(6), 2590–2596. https://doi.org/10.1002/2018GL077312

Connerney, J. E. P., Timmins, S., Herceg, M., & Joergensen, J. L. (2020). A Jovian magnetodisc model for the Juno era. *Journal of Geophysical Research: Space Physics*, *125*(10), e2020JA028138. https://doi.org/10.1029/2020JA028138

Connerney, J. E. P., Timmins, S., Oliverson, R. J., Espley, J. R., Joergensen, J. L., Kotsiaros, S., et al. (2022). A new model of Jupiter's magnetic field at the completion of Juno's prime mission. *Journal of Geophysical Research: Space Physics*, *127*(2), e2021JE007055. https://doi.org/10.1029/2021JE007055

Damiano, P. A., Delamere, P. A., Stauffer, B., Ng, C.-S., & Johnson, J. R. (2019). Kinetic simulations of electron acceleration by dispersive scale Alfvén waves in Jupiter's magnetosphere. *Geophysical Research Letters*, *46*(6), 3043–3051. https://doi.org/10.1029/2018GL081219

Dumont, M., Grodent, D., Radioti, A., Bonfond, B., & Gérard, J. C. (2014). Jupiter's equatorward auroral features: Possible signatures of magnetospheric injections. *Journal of Geophysical Research: Space Physics*, *119*(12), 10068–10077. https://doi.org/10.1002/2014JA020527

Gérard, J. C., Bonfond, B., Grodent, D., Radioti, A., Clarke, J. T., Gladstone, G. R., et al. (2014). Mapping the electron energy in Jupiter's aurora: Hubble spectral observations. *Journal of Geophysical Research: Space Physics*, *119*(11), 9072–9088. https://doi.org/10.1002/2014JA020514

Gérard, J. C., Gkouvelis, L., Bonfond, B., Grodent, D., Gladstone, G. R., Hue, V., et al. (2020). Spatial distribution of the Pedersen conductance in the Jovian Aurora from Juno-UVS spectral images. *Journal of Geophysical Research: Space Physics*, *125*(8), e2020JA028142. https://doi.org/10.1029/2020JA028142

Gérard, J. C., Gustin, J., Grodent, D., Delamere, P., & Clarke, J. T. (2002). Excitation of the FUV Io tail on Jupiter: Characterization of the electron precipitation. *Journal of Geophysical Research*, *107*(A11), 1319. https://doi.org/10.1029/2002JA009410

Gladstone, G. R., Versteeg, M. H., Greathouse, T. K., Hue, V., Davis, M. W., Gérard, J., et al. (2017). Juno-UVS approach observations of Jupiter's auroras. *Geophysical Research Letters*, *44*(15), 7668–7675. https://doi.org/10.1002/2017GL073377

Gordon, I. E., Rothamn, L. S., Hill, C., Kochanov, R. V., Tan, Y., Bernath, P. F., et al. (2017). The HITRAN2016 molecular spectroscopic database. *Journal of Quantitative Spectroscopy and Radiative Transfer*, *203*, 3–69. https://doi.org/10.1016/j.jqsrt.2017.06.038

Grodent, D. (2015). A brief review of ultraviolet auroral emissions on giant planets. *Space Science Reviews*, *187*(1–4), 23–50. https://doi.org/10.1007/s11214-014-0052-8

Grodent, D., Gérard, J.-C., Gustin, J., Mauk, B. H., Connerney, J. E. P., & Clarke, J. T. (2006). Europa's FUV auroral tail on Jupiter. *Geophysical Research Letters*, *33*(6), L06201. https://doi.org/10.1029/2005GL025487

Grodent, D., Waite, J. H., & Gérard, J. C. (2001). A self-consistent model of the Jovian auroral thermal structure. *Journal of Geophysical Research*, *106*(A7), 12739–13259. https://doi.org/10.1029/2000JA900129

Hess, S. L. G., Bonfond, B., Chantry, V., Gérard, J. C., Grodent, D., Jacobsen, S., & Radioti, A. (2013). Evolution of the Io footprint brightness II: Modeling. *Planetary and Space Science*, *88*, 76–85. https://doi.org/10.1016/j.pss.2013.08.005

Hess, S. L. G., Bonfond, B., & Delamere, P. A. (2013). How could the Io footprint disappear? *Planetary and Space Science*, *89*, 102–110. https://doi.org/10.1016/j.pss.2013.08.014

Hess, S. L. G., Delamere, P., Dols, V., Bonfond, B., & Swift, D. (2010). Power transmission and particle acceleration along the Io flux tube. *Geophysical Research Letters*, *115*(A6), A06205. https://doi.org/10.1029/2009JA014928

Hue, V., Greathouse, T. K., Bonfond, B., Saur, J., Gladstone, G. R., Roth, L., et al. (2019). Juno-UVS observation of the Io footprint during solar eclipse. *Journal of Geophysical Research: Space Physics*, *124*(7), 5184–5199. https://doi.org/10.1029/2018JA026431

Jakobsen, P., Ferruit, P., Alves de Oliveira, C., Arribas, S., Bagnasco, G., Barho, R., et al. (2022). The near-infrared spectrograph (NIRSpec) on the James Webb Space Telescope. I. Overview of the instrument and its capabilities. *Astronomy & Astrophysics*, *661*, A80. https://doi.org/10.1051/0004-6361/202142663

Johnson, R. E., Melin, H., Stallard, T. S., Tao, C., Nichols, J. D., & Chowdhury, M. N. (2018). Mapping H_3^+ temperatures in Jupiter's northern auroral ionosphere using VLT-CRIRES. *Journal of Geophysical Research: Space Physics*, *123*(17), 5990–6008. https://doi.org/10.1029/2018JA025511

Jones, S. T., & Su, Y.-J. (2008). Role of dispersive Alfvén waves in generating parallel electric fields along the Io-Jupiter fluxtube. *Journal of Geophysical Research*, *113*(A12), A12205. https://doi.org/10.1029/2008JA013512

Knowles, K. L., Stallard, T. S., O'Donoghue, J., Moore, L., Agiwal, O., Melin, H., et al. (2025). Magnetic silhouettes in Jupiter's non-auroral ionosphere. *Journal of Geophysical Research: Space Physics*, *130*(5), e2025JA033868. https://doi.org/10.1029/2025JA033868

Lam, H. A., Achilleos, N., Miller, S., Tennyson, J., Trafton, L. M., Geballe, T. R., & Ballester, G. E. (1997). Baseline spectroscopic study of the infrared auroras of Jupiter. *Icarus*, *127*(2), 379–393. https://doi.org/10.1006/icar.1997.5698

Lysak, R. L., & Song, Y. (2003). Kinetic theory of the Alfvén wave acceleration of auroral electrons. *Journal of Geophysical Research*, *108*(A4), 8005. https://doi.org/10.1029/2002JA009406

McComas, D. J., Alexander, N., Allegrini, F., Bagenal, F., Beebe, C., Clark, G., et al. (2017). The Jovian auroral distributions experiment (JADE) on the Juno mission to Jupiter. *Space Science Reviews*, *213*(1–4), 547–643. https://doi.org/10.1007/s11214-013-9990-9

Melin, H. (2025). h3ppy: An open-source python package for modelling and fitting H_3^+ spectra. *Journal of Open Source Software*, *10*(107), 7536. https://doi.org/10.21105/joss.07536

Melin, H., Fletcher, L. N., Hammel, H. B., Milam, S., Moore, L., Stallard, T. S., et al. (2025). The ionosphere of Uranus as revealed by JWST. *Geophysical Research Letters*, *52*(22), e2025GL118301. https://doi.org/10.1029/2025GL118301

Melin, H., Miller, S., Stallard, T., Smith, C., & Grodent, D. (2006). Estimated energy balance in the Jovian upper atmosphere during an auroral heating event. *Icarus*, *181*(1), 256–265. https://doi.org/10.1016/j.icarus.2005.11.004

Melin, H., O'Donoghue, J., Moore, L., Stallard, T. S., Fletcher, L. N., Roman, M. T., et al. (2024). Ionospheric irregularities at Jupiter observed by JWST. *Nature Astronomy*, *8*, 1000–1007. https://doi.org/10.1038/s41550-024-02305-9

Melin, H., Stallard, T. S., O'Donoghue, J., Moore, L., Tiranti, P. I., Knowles, K. L., et al. (2025). Temporal variability of the northern infrared Aurora of Jupiter as captured by JWST. *Journal of Geophysical Research: Space Physics*, *130*(8), e2025JA034261. https://doi.org/10.1029/2025JA034261

Migliorini, A., Dinelli, B. M., Moriconi, M. L., Altieri, F., Adriani, A., Mura, A., et al. (2019). H_3^+ characteristics in the Jupiter atmosphere as observed at limb with Juno/JIRAM. *Icarus*, *329*, 132–139. https://doi.org/10.1016/j.icarus.2019.04.003

Miller, S., Lam, H. A., & Tennyson, J. (1994). What astronomy has learned from observations of H_3^+. *Canadian Journal of Physics*, *72*(11–12), 760–771. https://doi.org/10.1139/p94-100

Miller, S., Stallard, T., Tennyson, J., & Melin, H. (2013). Cooling by H_3^+ emission. *Journal of Physical Chemistry A*, *117*(39), 9770–9777. https://doi.org/10.1021/jp312468b

Miller, S., Stallard, T. S., Melin, H., & Tennyson, J. (2010). H_3^+ cooling in planetary atmospheres. *Faraday Discussions*, *147*, 283–291. https://doi.org/10.1039/c004152c

Miller, S., Tennyson, J., Geballe, T. R., & Stallard, T. (2020). Thirty years of H_3^+ astronomy. *Reviews of Modern Physics*, *92*(3), 035003. https://doi.org/10.1103/RevModPhys.92.035003

Moirano, A., Bonfond, B., Sicorello, G., Vinesse, J., Szalay, J., Hue, V., et al. (2026). The vertical profile of the northern Io footprint auroral emission in the far-ultraviolet from Juno. Variability and energy spectrum of the precipitating electrons. *Astronomy & Astrophysics*, *706*, A205. https://doi.org/10.1051/0004-6361/202557463

Moirano, A., Mura, A., Adriani, A., Dols, V., Bonfond, B., Waite, J. H. E. A., et al. (2021). Morphology of the auroral tail of Io, Europa and Ganymede from JIRAM L-Band imager. *Journal of Geophysical Research: Space Physics*, *126*(9), e2021JA029450. https://doi.org/10.1029/2021JA029450

Moirano, A., Mura, A., Bonfond, B., Connerney, J. E. P., Dols, V., Grodent, D., et al. (2023). Variability of the auroral footprint of Io detected by Juno-JIRAM and modeling of the Io plasma torus. *Journal of Geophysical Research: Space Physics*, *128*(8), e2023JA031288. https://doi.org/10.1029/2023JA031288

Moore, L., Melin, H., O'Donoghue, J., Stallard, T. S., Moses, J. I., Galand, M., et al. (2019). Modelling H_3^+ in planetary atmospheres: Effects of vertical gradients on observed quantities. *Philosophical Transactions of the Royal Society A*, *377*(2154), 20190067. https://doi.org/10.1098/rsta.2019.0067

Moore, L., Mendillo, M., Müller-Wodarg, I. C. F., & Murr, D. L. (2004). Modeling of global variations and ring shadowing in Saturn's ionosphere. *Icarus*, *172*(2), 503–520. https://doi.org/10.1016/j.icarus.2004.07.007

Mura, A., Adriani, A., Connerney, J. E. P., Bolton, S., Altieri, F., Bagenal, F., et al. (2018). Juno observations of spot structures and a split tail in Io-induced aurorae on Jupiter. *Science*, *361*(6404), 774–777. https://doi.org/10.1126/science.aat1450

Mura, A., Moirano, A., Hue, V., Castagnoli, C., Migliorini, A., Altieri, F., et al. (2025). Vertical and temporal H_3^+ structure at the auroral footprint of Io. *The Planetary Science Journal*, *6*(2), 49. https://doi.org/10.3847/PSJ/ada6aa

Roberts, K., Moore, L., O'Donoghue, J., Melin, H., Stallard, T., Müller-Wodarg, I., et al. (2026). A global view of Jupiter's upper atmosphere through H_3^+. *The Astrophysics Journal*, *998*(1), L13. https://doi.org/10.3847/2041-8213/ae3c9b

Roth, L., Blöcker, A., de Kleer, K., Goldstein, D., Lellouch, E., Saur, J., et al. (2025). Mass supply from Io to Jupiter's magnetosphere. *Space Science Reviews*, *221*(13), 13. https://doi.org/10.1007/s11214-025-01137-x

Sánchez-López, A., López-Puertas, M., García-Comas, M., Funke, B., Fouchet, T., & Snellen, I. A. G. (2021). The CH_4 abundance in Jupiter's upper atmosphere. *Astronomy & Astrophysics*, *662*, A91. https://doi.org/10.1051/0004-6361/202141933

Saur, J. (2021). Chapter 36 - Overview of moon–magnetosphere interactions. In *Magnetospheres in the solar system*. American Geophysical Union. https://doi.org/10.1002/9781119815624.ch36

Saur, J., Grambusch, T., Duling, S., Neubauer, F. M., & Simon, S. (2013). Magnetic energy fluxes in sub-Alfvénic planet star and moon planet interactions. *Astronomy and Astrophysics*, *552*, A119. https://doi.org/10.1051/0004-6361/201118179

Stallard, T. S., Burrell, A. G., Melin, H., Fletcher, L. N., Miller, S., Moore, L., et al. (2018). Identification of Jupiter's magnetic equator through H_3^+ ionospheric emission. *Nature Astronomy*, *2*(10), 773–777. https://doi.org/10.1038/s41550-018-0523-z

Stallard, T. S., Moore, L., Melin, H., Agiwal, O., Chowdhury, M. N., Johnson, R. E., et al. (2025). JWST/NIRSpec detection of complex structures in Saturn's sub-auroral ionosphere and stratosphere. *Geophysical Research Letters*, *52*(17), e2025GL116491. https://doi.org/10.1029/2025GL116491

Steffl, A. J., Stewart, A. I., & Bagenal, F. (2004). Cassini UVIS observations of the Io plasma torus: I. Initial results. *Icarus*, *172*(1), 78–90. https://doi.org/10.1016/j.icarus.2003.12.027

Szalay, J. R., Allegrini, F., Bagenal, F., Bolton, S. J., Bonfond, B., Clark, G., et al. (2020). A new framework to explain changes in Io's footprint tail electron fluxes. *Geophysical Research Letters*, *47*(18), e2020GL089267. https://doi.org/10.1029/2020GL089267

Szalay, J. R., Bonfond, B., Allegrini, F., Bagenal, F., Bolton, S., Clark, G., et al. (2018). In situ observations connected to the Io footprint tail Aurora. *Journal of Geophysical Research: Planets*, *123*(11), 3061–3077. https://doi.org/10.1029/2018JE005752

Tao, C., Badman, S., & Fujimoto, M. (2011). UV and IR auroral emission model for the outer planets: Jupiter and Saturn comparison. *Icarus*, *213*(2), 581–592. https://doi.org/10.1016/j.icarus.2011.04.001

Wannawichian, S., Clarke, J. T., Bagenal, F., Smyth, W. H., Peterson, C. A., & Nichols, J. D. (2013). Longitudinal modulation of the brightness of Io's auroral footprint emission: Comparison with models. *Journal of Geophysical Research: Space Physics*, *118*(6), 3336–3345. https://doi.org/10.1002/jgra.50346

Wilson, R. J., Vogt, M. F., Provan, G., Kamran, A., James, M. K., Brennan, M., & Cowley, S. W. H. (2023). Internal and external Jovian magnetic fields: Community code to serve the magnetospheres of the outer planets community. *Space Science Reviews*, *219*(15), 15. https://doi.org/10.1007/s11214-023-00961-3